Probing the Electronic and Structural Properties of Chromium Oxide Clusters (CrO_3)$_n^-$ and (CrO_3)$_n$ (n = 1–5): Photoelectron Spectroscopy and Density Functional Calculations

ARTICLE *in* JOURNAL OF THE AMERICAN CHEMICAL SOCIETY · MAY 2008

Impact Factor: 12.11 · DOI: 10.1021/ja077984d · Source: PubMed

4 AUTHORS, INCLUDING:

David A Dixon
University of Alabama
766 PUBLICATIONS **22,181** CITATIONS
SEE PROFILE

Lai-Sheng Wang
Brown University
434 PUBLICATIONS **18,822** CITATIONS
SEE PROFILE

J|A|C|S
ARTICLES

Published on Web 03/08/2008

Probing the Electronic and Structural Properties of Chromium Oxide Clusters $(CrO_3)_n^-$ and $(CrO_3)_n$ (n = 1–5): Photoelectron Spectroscopy and Density Functional Calculations

Hua-Jin Zhai,[†] Shenggang Li,[‡] David A. Dixon,*[,‡] and Lai-Sheng Wang*[,†]

Department of Physics, Washington State University, 2710 University Drive, Richland, Washington 99354, Chemical & Materials Sciences Division, Pacific Northwest National Laboratory, MS K8-88, P.O. Box 999, Richland, Washington 99352, and Chemistry Department, The University of Alabama, Shelby Hall, Box 870336, Tuscaloosa, Alabama 35487-0336

Received October 17, 2007; E-mail: dadixon@bama.ua.edu; ls.wang@pnl.gov

Abstract: Photoelectron spectroscopy has been conducted for a series of $(CrO_3)_n^-$ (n = 1–5) clusters and compared with density functional calculations. Well-resolved photoelectron spectra were obtained for $(CrO_3)_n^-$ (n = 1–5) at 193 nm (6.424 eV) and 157 nm (7.866 eV) photon energies, allowing for accurate measurements of the electron binding energies, low-lying electronic excitations for n = 1 and 2, and the energy gaps. Density functional and molecular orbital theory (CCSD(T)) calculations were performed to locate the ground and low-lying excited states for the neutral clusters and to calculate the electron binding energies of the anionic species. The experimental and computational studies firmly establish the unique low-spin, nonplanar, cyclic ring structures for $(CrO_3)_n$ and $(CrO_3)_n^-$ for $n \geq 3$. The structural parameters of $(CrO_3)_n$ are shown to converge rapidly to those of the bulk CrO_3 crystal. The extra electron in $(CrO_3)_n^-$ ($n \geq 2$) is shown to be largely delocalized over all Cr centers, in accord with the relatively sharp ground-state photoelectron bands. The measured energy gaps of $(CrO_3)_n$ exhibit a sharp increase from n = 1 to n = 3 and approach to the bulk value of 2.25 eV at n = 4 and 5, consistent with the convergence of the structural parameters.

1. Introduction

Chromium oxides are of significant current interest due to their diverse technological applications. Chromium-based oxide catalysts are important in a number of industrial processes,[1] and CrO_2 is widely used in magnetic recording tapes and other magnetic layers.[2] The basis for Cr oxide catalysis over a wide spectrum of reactions is thought to lie in the variety of oxidation states, coordination environments, and degrees of polymerization that are available.[1] The magnetic properties of chromium oxides vary significantly with oxygen content: Cr_2O_3 is an insulator and is antiferromagnetic, whereas CrO_2 is a semiconductor and is ferromagnetic.[2] Gas-phase chromium oxide clusters provide controlled and well-defined models, which can be used to improve our mechanistic understanding of surface catalytic sites and the magnetic properties of chromium oxides at the molecular level. The size and composition dependence of structural, electronic, and magnetic properties of chromium oxide clusters may offer opportunities to tailor the chemical and physical properties of chromium oxides for further applications.

There have been a number of gas-phase experimental[3–13] and theoretical[9–12,14–16] studies on small chromium oxide clusters. Vibrationally resolved photoelectron spectroscopy (PES) was reported for CrO^- and CrO_2^-.[7] Magnetic properties of Cr_2O_n (n = 1–6) as a function of n were studied by density functional theory (DFT).[9,14] An early electron diffraction study of the vapor

[†] Washington State University and Pacific Northwest National Laboratory.
[‡] The University of Alabama.

(1) Weckhuysen, B. M.; Wachs, I. E.; Schoonheydt, R. A. *Chem. Rev.* **1996**, *96*, 3327.
(2) (a) de Groot, R. A.; Mueller, F. M.; van Engen, P. G.; Buschow, K. H. J. *Phys. Rev. Lett.* **1983**, *50*, 2024. (b) Korotin, M. A.; Anisimov, V. I.; Khomskii, D. I.; Sawatzky, G. A. *Phys. Rev. Lett.* **1998**, *80*, 4305.
(3) Ivanov, A. A.; Demidov, A. V.; Popenko, N. I.; Zasorin, E. Z.; Spiridonov, V. P. *J. Mol. Struct.* **1980**, *63*, 121.
(4) Hop, C. E. C. A.; McMahon, T. B. *J. Am. Chem. Soc.* **1992**, *114*, 1237.
(5) Fiedler, A.; Kretzschmar, I.; Schroder, D.; Schwarz, H. *J. Am. Chem. Soc.* **1996**, *118*, 9941.
(6) Chertihin, G. V.; Bare, W. D.; Andrews, L. *J. Chem. Phys.* **1997**, *107*, 2798.
(7) (a) Wenthold, P. G.; Gunion, R. F.; Lineberger, W. C. *Chem. Phys. Lett.* **1996**, *258*, 101. (b) Wenthold, P. G.; Jonas, K. L.; Lineberger, W. C. *J. Chem. Phys.* **1997**, *106*, 9961.
(8) Aubriet, F.; Muller, J. F. *J. Phys. Chem. A* **2002**, *106*, 6053.
(9) (a) Tono, K.; Terasaki, A.; Ohta, T.; Kondow, T. *Phys. Rev. Lett.* **2003**, *90*, 133402. (b) Tono, K.; Terasaki, A.; Ohta, T.; Kondow, T. *J. Chem. Phys.* **2003**, *119*, 11221.
(10) Bergeron, D. E.; Castleman, A. W., Jr.; Jones, N. O.; Khanna, S. N. *Nano Lett.* **2004**, *4*, 261.
(11) Gutsev, G. L.; Jena, P.; Zhai, H. J.; Wang, L. S. *J. Chem. Phys.* **2001**, *115*, 7935.
(12) Zhai, H. J.; Huang, X.; Waters, T.; Wang, X. B.; O'Hair, R. A. J.; Wedd, A. G.; Wang, L. S. *J. Phys. Chem. A* **2005**, *109*, 10512.
(13) Zhai, H. J.; Wang, L. S. *J. Chem. Phys.* **2006**, *125*, 164315.
(14) Reddy, B. V.; Khanna, S. N. *Phys. Rev. Lett.* **1999**, *83*, 3170.
(15) (a) Veliah, S.; Xiang, K. H.; Pandey, R.; Recio, J. M.; Newsam, J. M. *J. Phys. Chem. B* **1998**, *102*, 1126. (b) Xiang, K. H.; Pandey, R.; Recio, J. M.; Francisco, E.; Newsam, J. M. *J. Phys. Chem. A* **2000**, *104*, 990.
(16) Li, S. G.; Dixon, D. A. *J. Phys. Chem. A* **2006**, *110*, 6231.

phase of chromium trioxide determined the molecular structure of $(CrO_3)_4$ as a nonplanar cyclic ring with a puckering angle of ~39°.[3,17] A combined mass spectrometry and computational study showed evidence for two families of $Cr_mO_n^-$ clusters, each with distinct electronic and magnetic properties.[10] Nevertheless, definitive structural and electronic information on chromium oxide clusters is rather limited.

We are interested in elucidating the structural and electronic properties and chemical bonding in early transition metal oxide clusters and in developing cluster models for oxide surfaces and heterogeneous catalysts based on these species. Among our previous work, we conducted systematic PES studies to probe the electronic evolution as a function of oxygen content in two series of chromium oxide clusters: CrO_n^- (n = 1–5) and $Cr_2O_n^-$ (n = 1–7).[11–13] We also performed DFT calculations to predict the molecular and electronic structures, Brønsted basicities, and Lewis acidities of $(MO_3)_n$ (M = Cr, Mo, W; n = 1–6) clusters.[16] In the latter study, we predicted that the cyclic ring geometries are the global minima for $(CrO_3)_n$ (n = 3–6).[16]

PES of size-selected anions has proved to be a powerful technique to probe the electronic structure of atomic clusters and can yield direct experimental information about the energy gap for neutral clusters with closed-shell electron configurations.[18–20] However, PES of $(CrO_3)_n^-$ clusters is challenging due to their relatively high electron binding energies and sizable energy gaps. In this work, PES experiments were performed for $(CrO_3)_n^-$ (n = 1–5) at 193 nm (6.424 eV) and 157 nm (7.866 eV) photon energies. Well-resolved PES spectra were obtained, allowing for accurate measurement of the electron binding energies and the energy gaps. DFT calculations with different functionals and basis sets, as well as molecular orbital theory calculations at the CCSD(T) level, were performed on $(CrO_3)_n$ and $(CrO_3)_n^-$ (n = 1–5). The choice of functionals is based on our recent benchmark studies on the ground states of the $(MO_3)_{1,2}$ (M = Cr, Mo, W) clusters.[21] The combined experimental and theoretical study allows us (1) to benchmark computational methods for chromium oxide clusters, as Cr-based compounds have proved to be very challenging for computational chemistry[22] and there has been a lack of accurate experimental data for comparison; (2) to further establish the equilibrium geometries of $(CrO_3)_n$ and $(CrO_3)_n^-$ (n = 1–5), in particular, the unique low-spin nonplanar cyclic ring structures for the n = 3–5 species; and (3) to explore the evolution of the electronic structure and the energy gap for $(CrO_3)_n^-/(CrO_3)_n$ as a function of cluster size, in order to build up a connection between the finite $(CrO_3)_n$ clusters and the bulk CrO_3 crystal at the electronic and structural levels.

2. Experimental and Computational Methods

2.1. Photoelectron Spectroscopy. The experiment was carried out using a magnetic-bottle PES apparatus equipped with a laser vaporization cluster source, details of which have been described before.[23] Briefly, $Cr_mO_n^-$ clusters were produced by laser vaporization of a pure Cr disk target in the presence of a He carrier gas seeded with 0.5% O_2 and analyzed using a time-of-flight mass spectrometer. The $(CrO_3)_n^-$ (n = 1–5) clusters of interest were each mass-selected and decelerated before being photodetached. Two high photon energies were used in the experiment: 193 nm (6.424 eV) and 157 nm (7.866 eV). Effort was made to control the cluster temperatures and to choose colder clusters for photodetachment, which has proved essential for obtaining high quality PES data.[24] Photoelectrons were collected at nearly 100% efficiency by the magnetic-bottle and analyzed in a 3.5 m long electron flight tube. PES spectra were calibrated using the known spectrum of Au^-, and the energy resolution of the PES apparatus was $\Delta E_k/E_k \sim 2.5\%$, that is, ~25 meV for 1 eV electrons.

2.2. Computational Methods. DFT calculations were carried out for $(CrO_3)_n$ and $(CrO_3)_n^-$ (n = 1–5) to obtain the adiabatic and vertical electron detachment energies (ADEs and VDEs) for the anions. Our recent benchmark studies on the ground states of CrO_3^- and $Cr_2O_6^-$ have shown that accurate electron detachment energies can be obtained with DFT gradient-corrected exchange-correlation functionals without Hartree–Fock (HF) exchange (i.e., pure functionals), whereas the use of HF exchange (i.e., hybrid functionals) significantly overestimates the electron detachment energies.[21] Thus, we used the PW91[25,26] pure DFT exchange-correlation functional to optimize the geometries and calculate the harmonic frequencies. In these calculations, we used the aug-cc-pVDZ basis set for O[27] and the aug-cc-pVDZ-PP basis set for the effective core potential (ECP) for Cr (K.A. Peterson, personal communication); these basis sets will be collectively denoted as aD. The ECP basis set for Cr is constructed in the same manner as that for the second row transition metal atoms.[28] Single point energies were further calculated with the PW91[25,26] and BP86[29] pure DFT generalized gradient exchange-correlation functionals and the popular B3LYP[30] hybrid functional. These calculations were carried out with the aug-cc-pVTZ basis set for O and the aug-cc-pVTZ-PP basis sets for Cr; these basis sets will be denoted as aT. In addition, the energies were also calculated with the coupled cluster method at the CCSD(T)/aD level.[31] For open-shell anions, the R/UCCSD(T) approach was used, where a restricted open-shell Hartree–Fock (ROHF) calculation is initially performed and the spin constraint is then relaxed in the correlation treatment. The use of the relatively small basis set in these coupled cluster calculations is justified by the approximate cancelation of the basis set incompletion error in

(17) The puckering angle is defined as the dihedral angle between the O−Cr−O plane and the plane formed by the bridge oxygens.
(18) (a) Busani, R.; Folkers, M.; Cheshnovsky, O. *Phys. Rev. Lett.* **1998**, *81*, 3836. (b) Wang, X. B.; Ding, C. F.; Wang, L. S. *J. Chem. Phys.* **1999**, *110*, 8217. (c) Thomas, O. C.; Zheng, W.; Xu, S.; Bowen, K. H., Jr *Phys. Rev. Lett.* **2002**, *89*, 213403. (d) Li, J.; Li, X.; Zhai, H. J.; Wang, L. S. *Science* **2003**, *299*, 864. (e) Zhai, H. J.; Kiran, B.; Li, J.; Wang, L. S. *Nat. Mater.* **2003**, *2*, 827.
(19) Zhai, H. J.; Wang, L. S. *J. Am. Chem. Soc.* **2007**, *129*, 3022.
(20) Zhai, H. J.; Döbler, J.; Sauer, J.; Wang, L. S. *J. Am. Chem. Soc.* **2007**, *129*, 13270.
(21) Li, S.; Dixon, D. A. *J. Phys. Chem. A* **2007**, *111*, 11908.
(22) Dachsel, H.; Harrison, R. J.; Dixon, D. A. *J. Phys. Chem. A* **1999**, *103*, 152.
(23) (a) Wang, L. S.; Cheng, H. S.; Fan, J. *J. Chem. Phys.* **1995**, *102*, 9480. (b) Wang, L. S.; Wu, H. In *Advances in Metal and Semiconductor Clusters: Cluster Materials*; Duncan, M. A., Ed.; JAI Press: Greenwich, CT, 1998; Vol. 4, pp 299–343.
(24) (a) Wang, L. S.; Li, X. In *Clusters and Nanostructure Interfaces*; Jena, P., Khanna, S. N., Rao, B. K., Eds.; World Scientific: River Edge, NJ, 2000; pp 293–300. (b) Akola, J.; Manninen, M.; Hakkinen, H.; Landman, U.; Li, X.; Wang, L. S. *Phys. Rev. B* **1999**, *60*, R11297. (c) Wang, L. S.; Li, X.; Zhang, H. F. *Chem. Phys.* **2000**, *262*, 53. (d) Zhai, H. J.; Wang, L. S.; Alexandrova, A. N.; Boldyrev, A. I. *J. Chem. Phys.* **2002**, *117*, 7917.
(25) Burke, K.; Perdew, J. P.; Wang. Y. In *Electronic Density Functional Theory: Recent Progress and New Directions*; Dobson, J. F., Vignale, G., Das, M. P., Eds.; Plenum: New York, 1998.
(26) Perdew, J. P.; Wang, Y. *Phys. Rev. B* **1992**, *45*, 13244.
(27) Kendall, R. A.; Dunning, T. H., Jr.; Harrison, R. J. *J. Chem. Phys.* **1992**, *96*, 6796.
(28) Peterson, K. A.; Figgen, D.; Dolg, M.; Stoll, H. *J. Chem. Phys.* **2007**, *126*, 124101.
(29) (a) Becke, A. D. *Phys. Rev. A* **1988**, *38*, 3098. (b) Perdew, J. P. *Phys. Rev. B* **1986**, *33*, 8822.
(30) (a) Becke, A. D. *J. Chem. Phys.* **1993**, *98*, 5648. (b) Lee, C.; Yang, W.; Parr, R. G. *Phys. Rev. B* **1988**, *37*, 785.
(31) (a) Purvis, G. D.; Bartlett, R. J. *J. Chem. Phys.* **1982**, *76*, 1910. (b) Raghavachari, K.; Trucks, G. W.; Pople, J. A.; Head-Gordon, M. *Chem. Phys. Lett.* **1989**, *157*, 479. (c) Watts, J. D.; Gauss, J.; Bartlett, R. J. *J. Chem. Phys.* **1993**, *98*, 8718. (d) Bartlett, R. J.; Musial, M. *Rev. Mod. Phys.* **2007**, *79*, 291.

the calculation of the electron detachment energies to within ~0.1 eV for the ADE and ~0.2 eV for the VDE on the basis of our recent benchmark studies.[21]

For CrO_3 and Cr_2O_6, the lowest state of each spin and spatial symmetry was calculated with the above methods (self-consistent energies). For all clusters, we used the time-dependent DFT (TD-DFT)[32–35] method with the PW91, BP86, and B3LYP functionals to calculate the lowest 10 singlet and triplet excitation energies from the optimized neutral and anionic ground-state geometries for the closed-shell ground state of the neutral. An asymptotic correction[35] for the exchange-correlation functional was employed with the B3LYP functional, and no significant effect was observed on the transition energy for these relatively low excited states.

The DFT calculations were carried out with the Gaussian 03 program package.[36] For the pure DFT methods (PW91 and BP86), the density fitting approximation was employed to speed up the calculations.[37] The density fitting sets were automatically generated from the atomic orbital primitives. The CCSD(T) calculations were carried out with the MOLPRO 2006.1 program packages.[38] The TD-DFT calculations were performed with the NWChem 5.0 program packages.[39,40] The calculations were carried out on the Opteron-based Cray XD1 and Itanium 2-based Altix supercomputers at the Alabama Supercomputer Center, the Xeon-based Dell Linux cluster at the University of Alabama, the local Opteron-based Parallel Quantum Solutions Linux cluster, and the Itanium 2-based Linux cluster at the Molecular Science Computing Facility from the Pacific Northwest National Laboratory.

Multidimensional Franck–Condon factors (FCFs) for the vibronic transitions from the ground state of the anion to that of the neutral cluster were calculated within the harmonic approximation to simulate the PES spectra for CrO_3^- and $Cr_2O_6^-$. The program[41] was adapted from the work of Yang et al.[42] and the algorithms from Gruner and Brumer,[43] Ruhoff and Ratner,[44] and Hazra and Nooijen.[45] The PW91 equilibrium geometries, harmonic frequencies, and normal coordinates were used in these simulations. A Boltzmann distribution was used to account for the finite temperature effect with a Lorentzian line shape.

3. Experimental Results

The 193 and 157 nm PES spectra of $(CrO_3)_n^-$ (n = 1–5) are shown in Figure 1. Each species exhibits a weak, low binding energy band X, followed by an energy gap and a more intense band A at higher binding energies. For CrO_3^- and $Cr_2O_6^-$, numerous PES features are revealed beyond band A, which are labeled as B, C, and D in Figure 1. The PES bands appear to be well-defined with sharp onsets, allowing for accurate measurements of the ADEs and VDEs (Table 1) and the energy gap (Table 2). The ground-state ADEs and VDEs of CrO_3^- and $Cr_2O_6^-$ were reported previously from our vibrationally resolved PES spectra at 266 nm.[11,13] For $(CrO_3)_n^-$ (n = 3–5), no vibrational structure could be resolved and the ground-state ADE was determined by drawing a straight line along the leading edge of band X and then adding the instrumental resolution to the intersection with the binding energy axis. Although this is an approximate procedure, we were able to obtain a consistent ADE for band X of each species from the spectra taken at different photon energies. The ADEs (i.e., the electron affinities of the corresponding neutral species) thus determined are 3.66,[11] 4.25, 4.44, 4.61, and 4.80 eV for $(CrO_3)_n^-$ (n = 1–5), respectively, as given in Table 1. The small difference in the ADE of the dimer from our previously reported value (4.28 eV)[13] is based on reanalysis of the 266 nm PES data, in combination with the FCF simulations described below. Except for a large increase of 0.59 eV from n = 1 to 2, the electron affinities increase rather smoothly by 0.17–0.19 eV per CrO_3

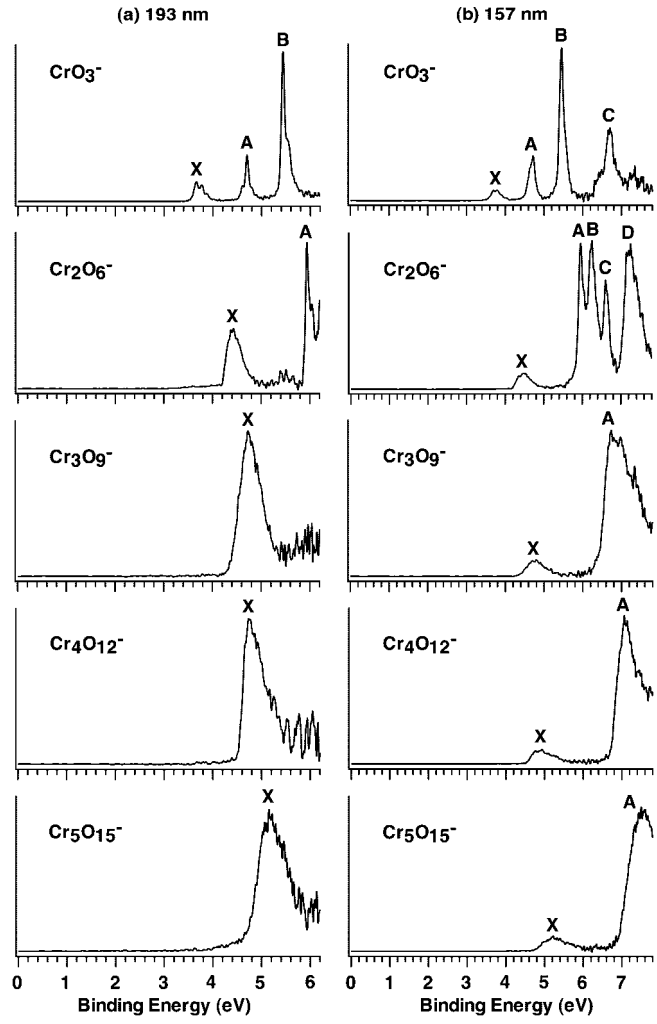

Figure 1. Photoelectron spectra of $(CrO_3)_n^-$ (n = 1–5) at (a) 193 nm (6.424 eV) and (b) 157 nm (7.866 eV).

(32) (a) Jamorski, C.; Casida, M. E.; Salahub, D. R. *J. Chem. Phys.* **1996**, *104*, 5134. (b) Bauernschmitt, R.; Ahlrichs, R. *Chem. Phys. Lett.* **1996**, *256*, 454. (c) Bauernschmitt, R.; Häser, M.; Treutler, O.; Ahlrichs, R. *Chem. Phys. Lett.* **1997**, *264*, 573.
(33) Hirata, S.; Head-Gordon, M. *Chem. Phys. Lett.* **1999**, *314*, 291.
(34) Casida, M. E.; Salahub, D. R. *J. Chem. Phys.* **2000**, *113*, 8918.
(35) (a) Hirata, S.; Zhan, C.-G.; Aprà, E.; Windus, T. L.; Dixon, D. A. *J. Phys. Chem. A* **2003**, *107*, 10154. (b) Zhan, C.-G.; Nicholas, J. A.; Dixon, D. A. *J. Phys. Chem. A* **2003**, *107*, 4184.
(36) Frisch, M. J.; et al. *Gaussian 03*, revision D.02; Gaussian, Inc.: Wallingford, CT, 2004.
(37) (a) Dunlap, B. I. *J. Chem. Phys.* **1983**, *78*, 3140. (b) Dunlap, B. I. *J. Mol. Struct. (THEOCHEM)* **2000**, *529*, 37.
(38) Werner, H.-J. *MOLPRO*, version 2006.1, a package of ab initio programs. See http://www.molpro.net.
(39) Bylaska, E. J.; et al. *NWChem, A Computational Chemistry Package for Parallel Computers* , version 5.0; Pacific Northwest National Laboratory: Richland, WA 99352–0999, 2006.
(40) Kendall, R. A.; Aprà, E.; Bernholdt, D. E.; Bylaska, E. J.; Dupuis, M.; Fann, G. I.; Harrison, R. J.; Ju, J.; Nichols, J. A.; Nieplocha, J.; Straatsma, T. P.; Windus, T. L.; Wong, A. T. *Comput. Phys. Commun.* **2000**, *128*, 260.
(41) Li, S. Ph.D. Thesis, University of Kentucky, August 2004.
(42) Yang, D.-S.; Zgierski, M. Z.; Rayner, D. M.; Hackett, P. A.; Mrtinex, A.; Salahub, D. R.; Roy, P. N.; Carrington, T., Jr *J. Chem. Phys.* **1995**, *103*, 5335.
(43) Gruner, D.; Brumer, P. *Chem. Phys. Lett.* **1987**, *138*, 310.
(44) Ruhoff, P. T.; Ratner, M. A. *Int. J. Quantum Chem.* **2000**, *77*, 383.
(45) Hazra, A.; Nooijen, M. *Int. J. Quantum Chem.* **2003**, *95*, 643.

Table 1. Experimental and Calculated Adiabatic and Vertical Electron Detachment Energies (ADEs and VDEs) for the X Band of the Photoelectron Spectra of $(CrO_3)_n^-$ (n = 1–5)

	ADE (eV)					VDE (eV)				
	exp.[a]	PW91[b]	BP86[b]	B3LYP[b]	CCSD(T)[c]	exp.[a]	PW91[b]	BP86[b]	B3LYP[b]	CCSD(T)[c]
CrO_3^-	3.66 (2)	3.51	3.57	4.08	3.70	3.77 (2)[d]	3.74	3.80	4.34	3.77
$(CrO_3)_2^-$	4.25 (5)[e]	4.26	4.31	4.57	4.24	4.45 (5)	4.39	4.43	4.85	4.37
$(CrO_3)_3^-$	4.44 (5)	4.30	4.35	4.85	4.23	4.75 (5)	4.52	4.55	5.18	4.54
$(CrO_3)_4^-$	4.61 (5)	4.70	4.75	4.90	4.74	4.80 (5)	4.78	4.82	5.08	4.89
$(CrO_3)_5^-$	4.80 (10)	4.87	4.92	5.11		5.17 (7)	4.97	5.01	5.33	

[a] Numbers in parentheses represent the experimental uncertainties. [b] Calculated with the aT basis sets using the PW91/aD geometries. [c] Calculated with the aD basis sets using the PW91/aD geometries. [d] Approximate value as assigned to the 1←0 transition in the 266 nm PES spectrum (dotted curve in Figure 5). The 0–0 and 1←0 transitions show roughly equal intensity, indicating significant geometric changes from the ground state of the anion to that of the neutral. The exact VDE may lie in between the 0–0 and 1←0 transitions, i.e., 3.66–3.77 eV. [e] From reanalysis of the 266 nm PES spectra in combination with the Franck–Condon simulation (Figure S1).

Table 2. Reorganization Energies (ΔE_{reorg}, eV) and Energy Gaps (ΔE_{gap}, eV) for $(CrO_3)_n$ (n = 1–5)

	ΔE_{reorg}[a]					ΔE_{gap}[b]						
	exp.[c]	PW91[d]	BP86[d]	B3LYP[d]	CCSD(T)[e]	exp.[c]	PW91(T)[f]	BP86(T)[f]	B3LYP(T)[f]	PW91(S)[g]	BP86(S)[g]	B3LYP(S)[g]
CrO_3	0.11 (3)[h]	0.23	0.23	0.26	0.07	1.04 (3)	1.24	1.37	1.60	1.38	1.51	1.75
$(CrO_3)_2$	0.20 (7)	0.13	0.12	0.28	0.13	1.68 (7)	1.64	1.64	2.13	1.76	1.76	2.32
$(CrO_3)_3$	0.31 (7)	0.22	0.20	0.33	0.31	2.02 (7)	2.17	2.20	2.54	2.35	2.36	2.96
$(CrO_3)_4$	0.19 (7)	0.08	0.07	0.18	0.15	2.14 (7)	2.06	2.08	2.52	2.25	2.25	2.94
$(CrO_3)_5$	0.37 (12)	0.10	0.09	0.22		2.15 (12)	2.04	2.07	2.47	2.17	2.17	2.89

[a] The reorganization energy is calculated as the difference between the ADE and VDE for the X band shown in Table 1. [b] The experimental energy gap is the difference between the ADEs of the X and A bands measured from the PES. The theoretical energy gap is the first excitation energy from the TD-DFT calculation with the aD basis set and the neutral ground-state geometry at the PW91/aD level. [c] Numbers in parentheses represent the experimental uncertainties. [d] Calculated with the aT basis set and the PW91/aD geometry. [e] Calculated with the aD basis set and the PW91/aD geometry. [f] The first excitation energy to the triplet states. [g] The first excitation energy to the singlet states. [h] Approximate value. See footnote d in Table 1.

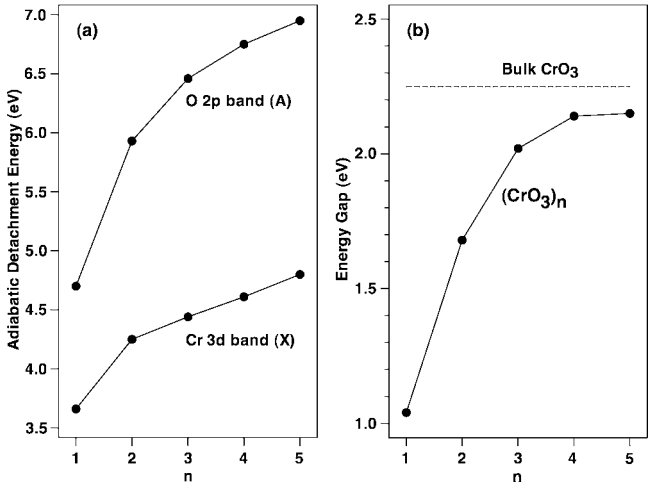

Figure 2. (a) Experimental adiabatic electron detachment energies for the Cr 3d-derived band (X) and O 2p-derived band (A). (b) The experimental energy gap, defined as the ADE difference of the X and A bands for $(CrO_3)_n$ (n = 1–5) as a function of the cluster size. For comparison, the bulk band gap of CrO_3 (2.25 eV; ref 55) is shown as a horizontal dashed line. Alternative bulk band gap values of 3.14 and 4.32 eV were also reported in the literature (refs 55 and 56).

unit and exhibit almost linear behavior for n = 2–5 as shown in Figure 2a.

The ground-state VDEs for CrO_3^- and $Cr_2O_6^-$ are defined by the most intense vibrational transition in the PES spectra as 3.77 and 4.45 eV, respectively,[11,13] where the VDE for CrO_3^- is reassigned to the 1←0 transition in the symmetric stretching progression (see footnote d in Table 1). The VDEs for $(CrO_3)_n^-$ (n = 3–5) are obtained from the peak maximum of band X as 4.75, 4.80, and 5.17 eV, respectively (Table 1). Similar to the trend for the ADEs, the VDEs also show a large increase of 0.68 eV from n = 1 to 2. The increase is smaller for n = 2–5 with an increase of 0.30 eV from n = 2 to 3, 0.05 eV from n = 3 to 4, and 0.37 eV from n = 4 to 5. The reorganization energy, defined as the difference between the ground-state ADE and VDE, was measured to be 0.11, 0.20, 0.31, 0.19, and 0.37 eV for $(CrO_3)_n^-$ (n = 1–5), respectively (Table 2). The reorganization energy characterizes the anion-to-neutral structural changes upon photodetachment and is relatively small for all species.

The ADEs for band A of $(CrO_3)_n^-$ (n = 1–5) were evaluated from the 157 nm spectra as 4.70 ± 0.02, 5.93 ± 0.03, 6.46 ± 0.05, 6.75 ± 0.05, and 6.95 ± 0.10 eV, respectively. The ADE difference between bands X and A defines the excitation energy from the singlet ground state to the lowest triplet excited state in the $(CrO_3)_n$ neutral species; these excitation energies were measured to be 1.04, 1.68, 2.02, 2.14, and 2.15 eV for n = 1–5, respectively (Table 2). The excitation energy shows a substantial increase only from n = 1 to 2 and n = 2 to 3, beyond which it levels off and approaches an asymptotic value (Figure 2b). In addition, the VDEs for band A of $(CrO_3)_n^-$ (n = 1–5) were measured from the 157 nm spectra as 4.70 ± 0.02, 5.98 ± 0.02, 6.72 ± 0.05, 7.05 ± 0.05, and 7.35 ± 0.10 eV, respectively.

Numerous higher excited states were resolved for CrO_3^- and $Cr_2O_6^-$ beyond band A (Figure 1). For CrO_3^-, a sharp and intense band B is located at a VDE of 5.43 eV, whereas band C at 6.69 eV appears weaker with broad shoulders. For $Cr_2O_6^-$, bands B and C have VDEs of 6.28 and 6.61 eV, respectively. Both bands appear sharp and well-resolved. Band D, centered at 7.22 eV, is broad and well-separated from band C.

4. Computational Results

Chromium and chromium oxide clusters impose a considerable challenge for the state-of-the-art quantum chemical methods.[22] On the basis of our recent benchmark study,[21] we chose

Table 3. Bond Lengths and Bond Angles Calculated at the PW91/aD Level for the Ground State of $(CrO_3)_n$ (n = 1–5), Estimated Asymptotic Values, and Comparison with the Experimental Structural Parameters of the CrO_3 Bulk Crystal[51]

	$n=1$	$n=2$	$n=3$	$n=4$	$n=5$	$n\rightarrow\infty$	bulk CrO_3
Cr═O (Å)	1.593	1.576	1.573/1.576	1.574	1.573/1.575	∼1.58	1.599
Cr−O (Å)		1.782	1.773	1.765	1.762	∼1.76	1.748
∠O═Cr═O (°)	113.3	110.9	110.4	109.7	109.2	∼109	109.5 (8)
∠O−Cr−O (°)		87.1	104.4	109.2	108.9	∼109	109.5 (8)
∠Cr−O−Cr (°)		92.9	120.4	134.7	141.5	∼145	143.0

to use the PW91 and BP86 exchange-correlation functionals to predict the electron detachment energies. We also report calculated detachment energies with the popular B3LYP functional as well as with the coupled cluster CCSD(T) method.

4.1. Equilibrium Geometries. Table 3 presents the bond lengths and bond angles calculated at the PW91/aD level for the ground states of $(CrO_3)_n$ (n = 1–5). Their structures are shown in Figure 3, and the Cartesian coordinates are listed in the Supporting Information. The CrO_3 molecules can combine to form a series of clusters with distinct arrangements,[16] the most stable of which are the ring structures for n = 3–5. The ground states of these clusters are quite symmetric with C_{nv} symmetry (Figure 3c−e); CrO_3 is nonplanar with C_{3v} symmetry (Figure 3a), and Cr_2O_6 has D_{2h} symmetry (Figure 3b). The ground states of $(CrO_3)_n$ are all closed-shell singlet states. As shown in Figure 3c, the six-member ring consisting of the Cr and bridge O atoms in Cr_3O_9 is nonplanar with a puckering angle of 27°.[17] The puckering angle slightly increases for the larger ring structures to 32 and 33° for n = 4 and 5, respectively. The calculated bond lengths and bond angles quickly converge to their asymptotic values as shown in Table 3, ∼1.58 and ∼1.76 Å for the Cr═O and Cr−O bond lengths, ∼109° for the O═Cr═O and O−Cr−O bond angles, and ∼145° for the Cr−O−Cr bond angle.

The ground-state structures of the anions calculated at the PW91/aD level are shown in Figure 4, and the geometric parameters are given in Table S1. The anion structures closely resemble those of the neutrals except that CrO_3^- is planar instead of pyramidal, and $Cr_3O_9^-$ and $Cr_5O_{15}^-$ have C_s symmetry instead of C_{nv} arising from Jahn–Teller distortions due to populating the e symmetry LUMO of the neutral with a single electron. As shown in Figure 4c, the six-member ring formed by the Cr and bridge O atoms is also nonplanar with a puckering angle of ∼22°, slightly smaller than that of Cr_3O_9. The puckering angle increases to ∼30° for the larger anionic ring structures. As shown in Figure 4c,d, two electronic states ($^2A'$ and $^2A''$) both with C_s symmetry arise from the Jahn–Teller distortion. The $^2A''$ state of $Cr_3O_9^-$ has essentially the same energy as that of the $^2A'$ state, although the former has one imaginary frequency of 113 cm^{-1}. In terms of the geometries, these two states can be considered to be formed by shrinking or expanding one of the angles of the equilateral triangle consisting of the Cr atoms in Cr_3O_9. Similar Jahn–Teller distortions occur for $Cr_5O_{15}^-$, and the ground state of $Cr_5O_{15}^-$ is also predicted to be a $^2A'$ state. The ground states of $Cr_2O_6^-$ and $Cr_4O_{12}^-$ are predicted to be ^2A_g and $^2B_2$, respectively, and have the same point group symmetry as those of the neutral clusters.

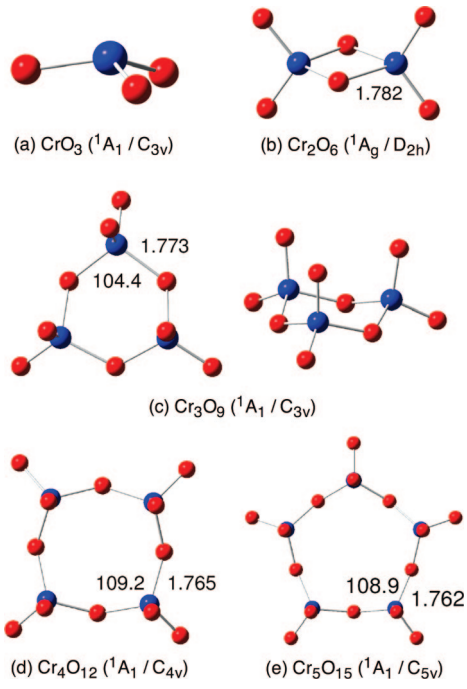

Figure 3. Molecular structures of the ground state of $(CrO_3)_n$ (n = 1–5) calculated at the PW91/aD level. The Cr−O bond lengths (Å) and the ∠O−Cr−O bond angles (°) are shown (Cr = blue; O = red).

4.2. Harmonic Frequencies. The calculated harmonic frequencies for the Cr═O and Cr—O stretches at the PW91/aD level are listed in Table S2 for $(CrO_3)_n$ and $(CrO_3)_n^-$ (n = 1–5). For CrO_3, the calculated Cr═O symmetric stretching frequency of 972 cm^{-1} is consistent with the experimental frequency of 890 ± 60 cm^{-1}.[11] For the dimer, the symmetric Cr−O stretching frequency of 748 cm^{-1} is consistent with the experimental value of 780 ± 50 cm^{-1}.[13] The Cr═O stretching frequencies in the neutral clusters range from 1020 to 1070 cm^{-1} for n > 1, and those in the anions range from 1000 to 1050 cm^{-1} for n > 2. Thus there is little change in these frequencies on addition of an electron, consistent with the small changes in geometry. The Cr−O stretching frequencies in the neutrals split into two groups, a group of higher frequencies (860−900 cm^{-1}) for n > 3 and a group of lower frequencies (500−640 cm^{-1}). The Cr−O stretching frequencies in the anions similarly split into two groups, a high frequency group (700−840 cm^{-1}) and a lower frequency group (500−550 cm^{-1}). The increase of the Cr−O stretching frequency as n increases is consistent with the Raman spectroscopic measurements of CrO_3 chains on a surface.[46]

4.3. Electron Binding Energies and Reorganization Energies. The ADEs and VDEs calculated at the PW91/aT, BP86/aT, B3LYP/aT, and CCSD(T)/aD levels with the PW91/aD geometries are compared to the experimental data in Table 1. The ADE is calculated as the energy difference between the ground state of the neutral and that of the anion, whereas the VDE is calculated as the electronic energy difference between the neutral at the anionic geometry and the anion itself. The calculated values at the PW91/aT and BP86/aT levels are close to each other, with the PW91/aT values slightly lower than the BP86/

(46) Weckhuysen, B. M.; Schoonheydt, R. A.; Jehng, J. M.; Wachs, I. E.; Cho, S. J.; Ryoo, R.; Kijlstra, S.; Poels, E. *J. Chem. Soc., Faraday Trans.* **1995**, *91*, 3245.

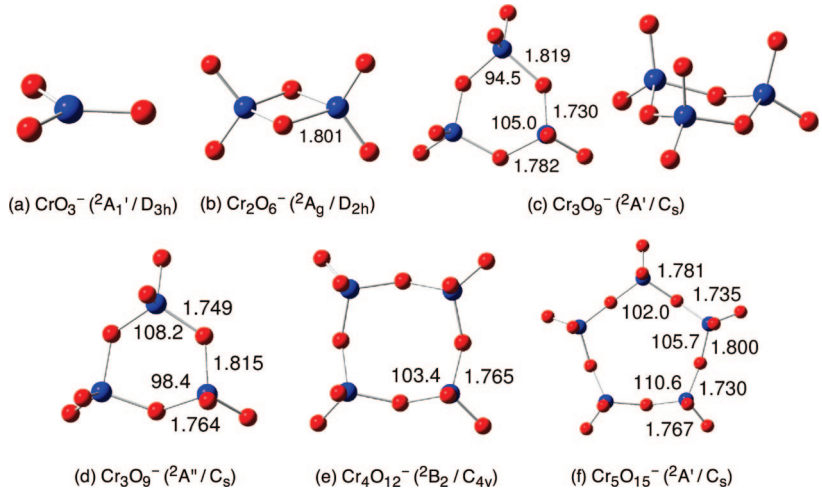

Figure 4. Molecular structures of the ground state of $(CrO_3)_n^-$ (n = 1–5) calculated at the PW91/aD level. The Cr−O bond lengths (Å) and the ∠O−Cr−O bond angles (°) are shown (Cr = blue; O = red).

Table 4. Experimental Vertical Electron Detachment Energies (VDEs) for CrO_3 and Cr_2O_6 Compared to the Self-Consistent DFT and CCSD(T) Results at the Anionic Geometries[a] and the Vertical Excitation Energies (Δ)[b] (All Energies Are in eV)

states	transition[c]	PW91VDE	PW91Δ	BP86VDE	BP86Δ	B3LYPVDE	B3LYPΔ	CCSD(T)VDE	CCSD(T)Δ	exp.VDE[d]	exp.Δ
CrO_3											
$^3A_2'$	$5a_1'$←$1a_2'$	4.64	0.90	4.68	0.88	4.96	0.62	4.72	0.95	A 4.70 (2)	0.93[e]
$^3A_2''$	$5a_1'$←$2a_2''$	5.61	1.87	5.64	1.84	5.64	1.30	5.48	1.71	B 5.43 (2)	1.66[e]
$^3E'$	$5a_1'$←$5e'$	5.29	1.55	5.34	1.54	5.68	1.34	5.61	1.84		
$^3E''$	$5a_1'$←$1e''$	6.76	3.02	6.80	3.00	6.92	2.58	6.67	2.90	C 6.69 (3)	2.92[e]
$^3A_1'$	$5a_1'$←$4a_1'$							6.94	3.17		
$^3E'$	$5a_1'$←$4e'$							7.68	3.91		
Cr_2O_6											
$^3B_{2u}$	$10a_g$←$6b_{2u}$	5.72	1.33	5.76	1.33	6.33	1.48	5.92	1.55	A 5.98 (2)	1.53
$^3B_{3g}$	$10a_g$←$2b_{3g}$	6.06	1.67	6.10	1.67	6.54	1.69	6.19	1.82		
$^3B_{1g}$	$10a_g$←$5b_{1g}$	5.97	1.58	6.01	1.58	6.56	1.71	6.28	1.91	B 6.28 (3)	1.83
$^3B_{1u}$	$10a_g$←$5b_{1u}$	6.40	2.01	6.44	2.01	6.86	2.01	6.68	2.31	C 6.61 (3)	2.16
^3A_g	$10a_g$←$9a_g$	6.90	2.51	6.94	2.51	7.58	2.73	7.27	2.90	D 7.22 (5)	2.77
$^3B_{2g}$	$10a_g3b_{2g}$	7.07	2.68	7.11	2.68	7.65	2.80	7.33	2.96		
$^3B_{3u}$	$10a_g$←$7b_{3u}$	7.26	2.87	7.30	2.87	7.90	3.05	7.68	3.31	—	—

[a] Calculated as the electronic energy difference between the excited state at the anionic geometry and the ground state of the anion. [b] Calculated as the VDE difference between the excited state and the ground state of the neutral. [c] The 1s2s2p orbitals on Cr are excluded in counting the orbitals. The electron configuration for the ground state of CrO_3 is $\cdots(4e')^4(1e'')^4(4a_1')^2(2a_2'')^2(5e')^4(1a_2')^2$ in D_{3h} symmetry. That of Cr_2O_6 is $\cdots(7a_g)^2(4b_{2u})^2(2b_{2g})^2(5b_{3u})^2(1b_{3g})^2(4b_{1g})^2(4b_{1u})^2$ $(8a_g)^2(6b_{3u})^2(1a_u)^2(7b_{3u})^2(3b_{2g})^2(9a_g)^2(5b_{2u})^2(5b_{1u})^2(2b_{3g})^2(5b_{1g})^2(6b_{2u})^2$ in D_{2h} symmetry. [d] Numbers in parentheses represent the experimental uncertainties. [e] Approximate value. See note d in Table 1.

aT values by ~0.05 eV. These values are also remarkably close to the CCSD(T)/aD data, whereas the B3LYP/aT data are significantly larger.

The calculated reorganization energies are compared with the experimental data in Table 2. For n = 1, the reorganization energies calculated at the PW91/aT, BP86/aT, and B3LYP/aT levels are consistent with that calculated at the CCSD(T)/CBS level (0.20 eV);[21] however, that calculated at the CCSD(T)/aD level is too low by 0.13 eV compared to the CCSD(T)/CBS value. For Cr_2O_6, the PW91/aT, BP86/aT, and CCSD(T)/aD results are very similar, whereas the B3LYP/aT value is too high. For the larger species, the PW91/aT and BP86/aT results give lower reorganization energies than the CCSD(T)/aD and experimental values, and the B3LYP/aT results are close to those of CCSD(T)/aD.

4.4. Excitation Energies and Energy Gaps. Table 2 also lists the calculated energy gaps (i.e., the excitation energies to the lowest triplet states) for $(CrO_3)_n$ (n = 1–5). We have previously shown that the first triplet state has a lower excitation energy than the first singlet excited state for $(MO_3)_n$ (M = Cr, Mo, W; n = 1–6).[16] The energy gaps at the PW91/aD and BP86/aD TD-DFT levels are, in general, nearly the same, except for CrO_3, where the BP86/aD value is ~0.1 eV higher than the PW91/aD value. We also calculated the singlet excitation energies with the TD-DFT method (Table 2). The first singlet excitation energies at the PW91/aD level are 0.1–0.2 eV higher than the first triplet excitation energies. The energy gaps predicted from the TD-DFT calculations at the anion geometries (Table S3) with the BP86 and PW91 functionals differ from the experimental values by up to 0.6 eV. The TD-DFT calculations with the B3LYP functional generate much larger energy gaps compared to those with the PW91 and BP86 functionals.

In order to benchmark the TD-DFT method, we also calculated the energies of the appropriate states of the neutral species at the geometry of the anion for CrO_3 and Cr_2O_6 with different functionals at the DFT and the CCSD(T) levels; this method will be labeled as self-consistent DFT, and the results are given in Table 4 and as Supporting Information (Tables S4−S10). Unlike TD-DFT, the self-consistent DFT approach is limited to the lowest energy state of each spin and spatial symmetry, as are direct CCSD(T) calculations of the energy differences. The self-consistent DFT results are in reasonable agreement with the CCSD(T) results for CrO_3 and Cr_2O_6. The CCSD(T) results enable qualitative assignments of the experi-

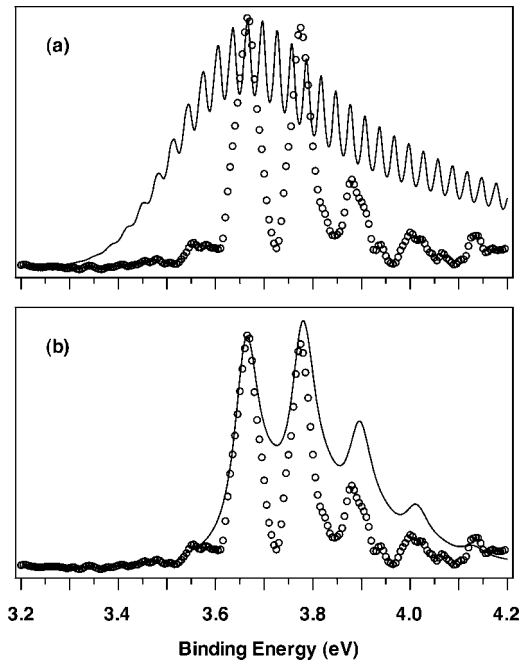

Figure 5. Franck–Condon simulations of the 266 nm photoelectron spectrum of CrO_3^- at the PW91/aD level: (a) $^1A_1 \leftarrow {}^2A_1'$ (planar anion to nonplanar neutral); (b) $^1A_1' \leftarrow {}^2A_1'$ (planar anion to planar neutral). Parameters for the simulations: full width at half-maximum (fwhm), 20 meV for (a) and 60 meV for (b); vibrational temperature, 100 K. The highest intensity peak in simulation is aligned to 0–0 transition of the experimental spectrum.

mental PES data (Table 4) for CrO_3 and Cr_2O_6. For CrO_3, TD-DFT calculations with all three functionals give the same ordering of excited states, but the TD-DFT results do not agree with the CCSD(T) ordering just as found for the self-consistent DFT calculations. The B3LYP TD-DFT VDEs are, in general, in worse agreement with the CCSD(T) results than those with the other functionals. For Cr_2O_6, the ordering of the states can depend on the functional (Table S4). We also calculated VDEs and energy gaps for states that do not involve the LUMO. As shown in Tables S7 and S8, the optical spectrum of the neutral for both CrO_3 and Cr_2O_6 will contain additional peaks relative to those found from the PES experiments.

5. Comparison Between Experiment and Theory for the Monomer and Dimer

5.1. Benchmarks of the Theoretical Methods. The PES data can be used to benchmark the theoretical methods and confirm the cluster structures. Our recent benchmark study shows that, for CrO_3^- and $Cr_2O_6^-$, B3LYP/aT and CCSD(T) at the complete basis set (CBS) limit overestimate the VDEs by ~0.7 and ~0.3 eV, respectively, whereas most of the exchange-correlation functionals without HF exchange give VDEs within 0.1 eV of the experiment.[21]

Compared to the experimental VDEs (Table 1), the calculated VDEs at the PW91/aT and BP86/aT levels are within the experimental error for CrO_3^-, $Cr_2O_6^-$, and $Cr_4O_{12}^-$ and lower by ~0.2 eV for $Cr_3O_9^-$ and $Cr_5O_{15}^-$. The calculated VDEs at the B3LYP/aT level are higher than the experimental values by ~0.6 eV for CrO_3^-, ~0.4 eV for $Cr_2O_6^-$ and $Cr_3O_9^-$, ~0.3 eV for $Cr_4O_{12}^-$, and less than 0.2 eV for $Cr_5O_{15}^-$. The calculated VDEs at the CCSD(T)/aD level are within the experimental error for CrO_3^-, $Cr_2O_6^-$, and $Cr_4O_{12}^-$ and lower than the experimental value by ~0.2 eV for $Cr_3O_9^-$. Thus, the performances of the PW91 and BP86 functionals are not quite uniform for all of the clusters but are superior to the B3LYP functional in all cases. For the CCSD(T)/aD method, cancelation of errors significantly improved its performance considering that CCSD(T)/ CBS overestimates the VDE of CrO_3^- by ~0.2 eV and that of $Cr_2O_6^-$ by ~0.3 eV. In addition, the agreement between theory and experiment is better for $n = 1$, 2, and 4 than for $n = 3$ and 5 as the ground states of $Cr_3O_9^-$ and $Cr_5O_{15}^-$ are subject to the Jahn–Teller effect and first-order spin–orbit splitting. Similar conclusions are obtained in comparing the experimental and calculated ADEs. The B3LYP values exhibit the worst agreement, the PW91 and BP86 values are within 0.15 eV of the experiment, and the CCSD(T)/aD results are within 0.2 eV of the experiment.

The calculated reorganization energies (Table 2) for CrO_3^- are similar at the PW91/aT, BP86/aT, and B3LYP/aT levels and are too large compared to the experiment, with the CCSD(T)/aD value being too small by 0.04 eV. For $Cr_2O_6^-$, the PW91/aT, BP86/aT, and CCSD(T)/aD results are similar, whereas the B3LYP/aT value is too high. All values are within ~0.1 eV of the experimental data. For the larger clusters, PW91/aT and BP86/aT underestimate the reorganization energy by ~0.1 eV for $n = 3$ and 4 and by ~0.3 eV for $n = 5$, whereas the B3LYP/aT and CCSD(T)/aD values are within the experimental error.

In terms of the energy gaps (Table 2), the results at the PW91/aD level using the neutral geometries are within the experimental error for Cr_2O_6, Cr_4O_{12}, and Cr_5O_{15} and slightly higher by ~0.2 eV for CrO_3 and Cr_3O_9. The energy gaps calculated at the B3LYP/aD level are higher than the experimental values by 0.3–0.5 eV. The energy gaps calculated with the TD-DFT method at the anionic equilibrium geometries are much lower than those calculated at the neutral geometries, by 0.2–0.3 eV for $n = 1$, 2 and 4, 0.5–0.6 eV for $n = 3$ and 5 at the PW91/aD level, and are not in good agreement with the experimental values except for $n = 1$ (Table S3).

5.2. On Higher Excited States of CrO_3 and Cr_2O_6. To benchmark the TD-DFT method, results for higher excited states of CrO_3 and Cr_2O_6 are shown in Tables 4 and S4. The B3LYP functional at the TD-DFT and self-consistent DFT levels does not work as well in comparison to the CCSD(T) method and experiment. In Table 4, the self-consistent DFT data are compared with those from CCSD(T). For the A band of CrO_3, the PW91, BP86, and CCSD(T) values for the VDE are all within the experimental uncertainty, whereas the B3LYP result is more than 0.25 eV higher. For the A band of Cr_2O_6, the PW91 and BP86 results for the VDE are 0.26 and 0.22 eV smaller than the experimental value, respectively, and the B3LYP value is 0.35 eV too high. The CCSD(T) result for the VDE of the A band is in excellent agreement with the experiment. The excitation energies are in error by about 0.2 eV for the BP86 and PW91 functionals, and the B3LYP and CCSD(T) values are in excellent agreement with the experiment.

Since the CCSD(T) method gives good agreement for band A of CrO_3 and Cr_2O_6, we used these calculations to assign the other bands (Table 4). Because of the presence of degenerate orbitals in CrO_3, the self-consistent calculations are difficult for some states. For band B of CrO_3, the agreement between the CCSD(T) and experimental VDEs is within 0.05 eV. Thus the B band is assigned to the detachment from the $2a_2''$ orbital. The B band should also contain contributions from detachment from the $5e'$ orbital; the calculated VDE from this detachment channel is very close to that from the $2a_2''$ orbital.

The C band is assigned to detachment from the 1e″ orbital. Two other detachment channels are also predicted at VDEs of 6.94 and 7.68 eV, which should correspond to the weaker signals observed in the higher binding side in the 157 nm spectrum (Figure 1b). For Cr_2O_6, the B band can be assigned to detachments from both the $5b_{1g}$ and $2b_{3g}$ orbitals. The C band can be assigned to detachment from the $5b_{1u}$ orbital. The D band should correspond to detachment from both $9a_g$ and $3b_{2g}$ orbitals, whose VDEs are predicted to differ by 0.06 eV. Overall, all the observed PES bands for CrO_3^- and $Cr_2O_6^-$ can be assigned and understood on the basis of our CCSD(T) calculations.

5.3. Franck–Condon Factor Simulations. Franck–Condon factor simulations were performed for the ground-state transition of CrO_3^- for two cases: $^1A_1 \leftarrow {}^2A_1'$ (i.e., planar anion to nonplanar neutral) and $^1A_1' \leftarrow {}^2A_1'$ (i.e., planar anion to planar neutral) at the PW91/aD level, as shown in Figure 5. When simulating the spectrum for the $^1A_1' \leftarrow {}^2A_1'$ transition, the imaginary frequency was substituted with its absolute value. The simulated spectrum for the $^1A_1 \leftarrow {}^2A_1'$ transition is dominated by an extremely long progression of the inversion vibration with a frequency of 242 cm^{-1} and a ratio of ~8 for the intensity of the 1←0 transition to that of the 0–0 transition, which totally disagrees with the observed spectrum. The simulated spectrum for the $^1A_1' \leftarrow {}^2A_1'$ transition, however, is dominated by a very short progression of the symmetric Cr═O stretching vibration with a frequency of 942 cm^{-1}, which matches the experimental spectrum. The experimental observation of a very short progression of the symmetric stretching vibration is in accord with the fact that there is a significant difference in the bond length of the anion and the neutral of ~0.04 Å with that in the anion being longer. The negligible Franck–Condon activity in the bending mode suggests the presence of a very low inversion barrier in the neutral, which is calculated to be 0.5 kcal/mol at CCSD(T)/aD level.

The simulated spectrum for the ground-state transition of $Cr_2O_6^-$ ($^1A_g \leftarrow {}^2A_g$) is much broader, agreeing well with the experimental spectrum (Figure S1). Several vibrational modes show fairly strong intensity in the simulated spectrum: the Cr−O−Cr symmetric bending mode (273 cm^{-1}) and the Cr−O and Cr═O symmetric stretching modes (748 and 1054 cm^{-1}). A reanalysis of the 266 nm PES spectrum[13] in combination with the FCF simulation allows for a slight refinement of the ADE of $Cr_2O_6^-$ as 4.25 ± 0.05 eV (Table 1).

6. Discussion

6.1. Reorganization Energy, Frontier Molecular Orbitals, and Electron Delocalization. The observed reorganization energies for $(CrO_3)_n^-$ (n = 1–5) as shown in Table 2 are relatively small in comparison to our previous PES works on other oxide clusters, such as $(SiO_2)_n^-$ and $(TiO_2)_n^-$.[19,47] For example, a reorganization energy of ~1.0 eV was obtained for $(TiO_2)_5^-$,[19] and a value of ~1.6 eV was predicted for $(SiO_2)_3^-$ from ab initio calculations.[47] In a very recent PES study, we showed evidence for a correlation between reorganization energies and electron delocalization/localization in $(V_2O_5)_n^-$ (n = 2–4) polyhedral cage clusters.[20,48] A localized electron significantly alters the local bonding environment around a metal center and hence induces large geometric changes upon photodetachment. The small reorganization energies observed for $(CrO_3)_n^-$ (n = 1–5) are consistent with the extra electron in the anions being highly delocalized over the metal centers (Figures 6 and 7). There is a size dependence of the reorganization energy, in which $Cr_3O_9^-$ and $Cr_5O_{15}^-$ show larger values than their neighbors (Table 2). This trend is also predicted by the calculations at the B3LYP/aT and CCSD(T)/aD levels and is due to the Jahn–Teller effect in $Cr_3O_9^-$ and $Cr_5O_{15}^-$.

Figure 6 shows the HOMO and LUMO for the $(CrO_3)_n$ (n = 1–5) clusters. The HOMO of $(CrO_3)_n$ is dominated by the 2pπ orbitals on the μ-oxo (terminal) oxygen. It is a degenerate orbital for $n \geq 3$. The LUMO is dominated by the Cr 3d orbitals. For $n = 2$, both the LUMO and the next LUMO (LUMO+1) are nondegenerate due to the D_{2h} symmetry. For $n = 3$ and 5, the LUMO is a degenerate orbital, whereas the LUMO+1 is a nondegenerate orbital. For $n = 1$ and 4, the LUMO is a nondegenerate orbital, whereas the LUMO+1 is a degenerate orbital. There is a substantial energy difference between the LUMO and the LUMO+1, 33.9 kcal/mol (1.47 eV), 22.4 kcal/mol (0.97 eV), 15.0 kcal/mol (0.65 eV), 11.7 kcal/mol (0.51 eV), and 18.0 kcal/mol (0.78 eV) for n = 1–5, respectively, from the PW91 calculations. As we have shown recently for M_3O_9 and $M_3O_9^-$ (M = Mo and W),[49] Jahn–Teller distortion can reduce the molecular symmetry when the degenerate orbital of the neutral is singly occupied by an additional electron to form the anion. We note that the observed small variation in reorganization energies suggests that the Jahn–Teller distortion in $Cr_3O_9^-$ and $Cr_5O_{15}^-$ is relatively small just as found computationally.

6.2. Equilibrium Geometries and Cluster-to-Bulk Structural Evolution. The ground state of CrO_3 was predicted to be pyramidal (Figure 3a), whereas that of CrO_3^- was predicted to be planar (Figure 4a). The pyramidal angle for CrO_3 was calculated to be 105.3° at the PW91/aD level, quite different from that of CrO_3^- (90.0°).[50] Planar CrO_3 (the $^1A_1'$ state) was predicted to be a transition state for inversion with an imaginary frequency of 185 cm^{-1} at the PW91/aD level and was also predicted to be a transition state at the B3LYP/aD, BP86/aD, and CCSD(T)/aT levels.[21] The calculated inversion barrier for CrO_3 is 3.1, 3.3, 1.3, and 0.5 kcal/mol at the PW91/aT, BP86/aT, B3LYP/aT, and CCSD(T)/aD levels, respectively, with zero point energy (ZPE) corrections included. We previously obtained a ZPE-corrected value of 1.5 kcal/mol at the CCSD(T)/CBS level.[21] For $Cr_2O_6^-$, we recently found that the B3LYP functional yields a structure with C_{2v} symmetry (the $^2A_1$ state), whereas the BP86 and PW91 functionals yield a structure with D_{2h} symmetry (the ^2A_g state).[21] At the CCSD(T)/aD level, the $^2A_1$ state was predicted to be ~0.3 kcal/mol lower in energy than the ^2A_g state excluding the ZPE corrections.

The variation of the geometry parameters for the anions as a function of cluster size is obscured by the Jahn–Teller effect in $Cr_3O_9^-$ and $Cr_5O_{15}^-$ (Table S1). Excluding these two clusters, the Cr═O and Cr−O bond lengths and O═Cr═O bond angle appear to converge to asymptotic values of ~1.58 and ~1.76 Å and ~110°, respectively, although the O−Cr−O and Cr−O−Cr bond angles are probably not quite fully converged. The calculated structural properties of the $(CrO_3)_n$ (n = 1–5) clusters are given in Table 3. With increasing cluster size, the structural

(47) Wang, L. S.; Nicholas, J. B.; Dupuis, M.; Wu, H.; Colson, S. D. *Phys. Rev. Lett.* **1997**, *78*, 4450.
(48) (a) Vyboishchikov, S. F.; Sauer, J. *J. Phys. Chem. A* **2001**, *105*, 8588. (b) Asmis, K. R.; Santambrogio, G.; Brummer, M.; Sauer, J. *Angew. Chem., Int. Ed.* **2005**, *44*, 3122.
(49) Li, S.; Dixon, D. A. *J. Phys. Chem. A*, **2007**, *111*, 11093.
(50) The pyramidal angle is defined as the angle between the C_3 axis and the X−Y bond in XY_3 with C_{3v} symmetry. For XY_3 with D_{3h} symmetry, the pyramidal angle is 90°.

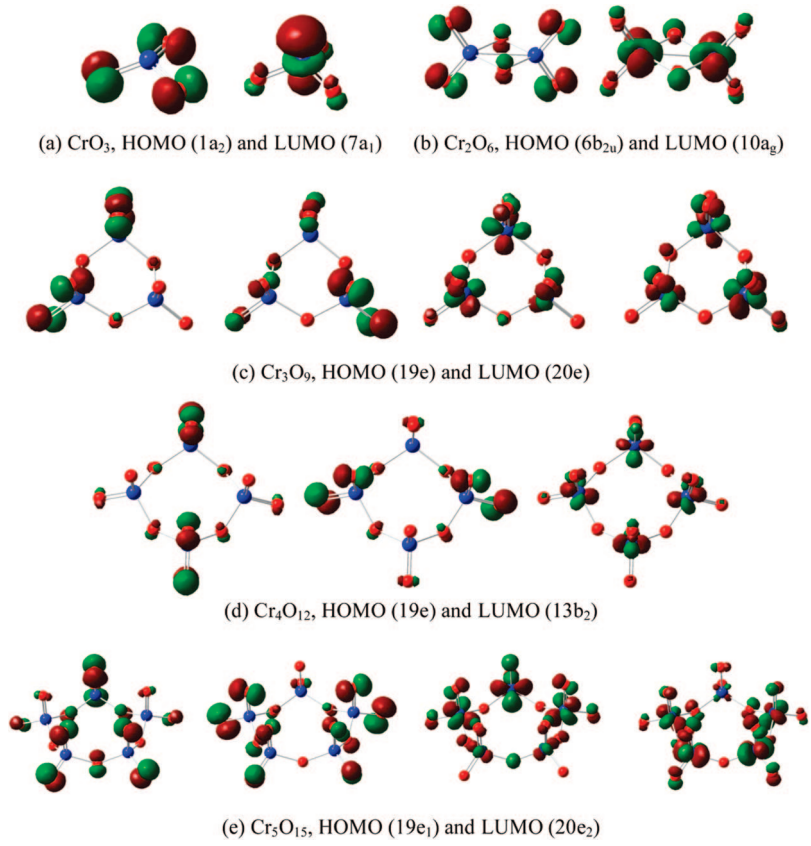

Figure 6. The highest occupied and lowest unoccupied molecular orbitals (HOMO and LUMO) for the ground state of $(CrO_3)_n$ (n = 1–5).

parameters of the $(CrO_3)_n$ clusters quickly approach those of bulk CrO_3. For example, the Cr═O bond length is close to that of the bulk even for the dimer (n = 2), and it appears virtually constant for n = 2–5. The Cr−O bond length shrinks slightly from n = 2 to n = 3 to n = 4 and becomes constant for $n \geq 4$. The tetrahedral bond angles (∠O═Cr═O and ∠O−Cr−O) in the clusters follow a similar trend and rapidly converge to the ideal tetrahedral bond angle of 109.5°. Due to the puckering angle that converges to about 30°, the bridging bond angle (∠Cr—O—Cr) in $(CrO_3)_n$ varies from 120° → 135° → 142° (n = 3–5). It reaches a maximum of about 145° instead of 180°, remarkably similar to the ∠Cr−O−Cr bridging bond angle of 143° in the bulk.[51]

The asymptotic values for the anions and the neutrals are essentially the same (Tables 3 and S1). This can be explained by considering the SOMO and electron spin density for the $(CrO_3)_n^-$ anions, which is dominated by the d orbitals on Cr and largely delocalized on all of the Cr centers for $n \geq 2$ (Figure 7). For n = 2 and 4, the spin density on all the Cr centers is identical, as shown in Figure 7b,d. For n = 3, the spin density is localized on one of the Cr centers to some degree, although there is substantial electron density on the other two Cr centers. For n = 5, the spin density on three of the Cr centers is significantly higher than the other two. We note that, as the other state resulting from the Jahn–Teller distortion lies very close in energy, the electron density is likely to be more delocalized than those depicted in Figure 7c,e for n = 3 and 5. In any case, the negative charge on $(CrO_3)_n^-$ is well delocalized for $n \geq 2$. Thus, its effect on the cluster geometry diminishes as n increases, and the asymptotic values of the geometries of the anions are identical to those of the neutral clusters.

The nonplanar cyclic ring equilibrium geometries are unique for the $(CrO_3)_n^-$ and $(CrO_3)_n$ (n = 3–5) clusters, which can be viewed as tetrahedral CrO_4 units fused together by sharing corners, each Cr center being tetra-coordinated by two terminal O atoms (Cr═O) and two bridging O atoms (Cr−O). In the case of the dimer, the structure is constrained to have two bridging O atoms between the Cr atoms, whereas in the larger clusters, there is only one bridging O atom between a pair of Cr atoms. In a similar fashion, the bulk CrO_3 crystal is composed of infinite linear chains of corner-sharing CrO_4 tetrahedra, in which the adjacent chains are held together by van der Waals forces.[51] The structural connection makes the $(CrO_3)_n$ and $(CrO_3)_n^-$ clusters ideal models to explore the molecular to bulk structural transition.

We compare the current equilibrium geometries with those of a previous DFT study.[10] In terms of the calculated electron affinities, the values in ref 10 for $(CrO_3)_n$ (n = 3–5) are 4.32, 4.62, and 4.92 eV, respectively, in excellent agreement with those from the current DFT calculations (4.30, 4.70, and 4.87 eV) and the experiment (4.44, 4.61, and 4.80 eV). However, the equilibrium geometries from ref 10 are very different from those shown in Figures 3 and 4. The current geometries are of C_{nv} symmetry for the neutrals and C_{nv} or C_s for the anions, whereas those from ref 10 appear to possess D_{nh} symmetry for both neutrals and anions. Our calculations indicate that at least the D_{3h} geometry is a third-order saddle point for $(CrO_3)_3$. It is unclear whether frequency calculations were done in ref 10 to ascertain that all structures are true minima. Furthermore, as discussed above, a substantial puckering angle of ∼39° was determined for $(CrO_3)_4$ by gas phase electron diffraction,[3]

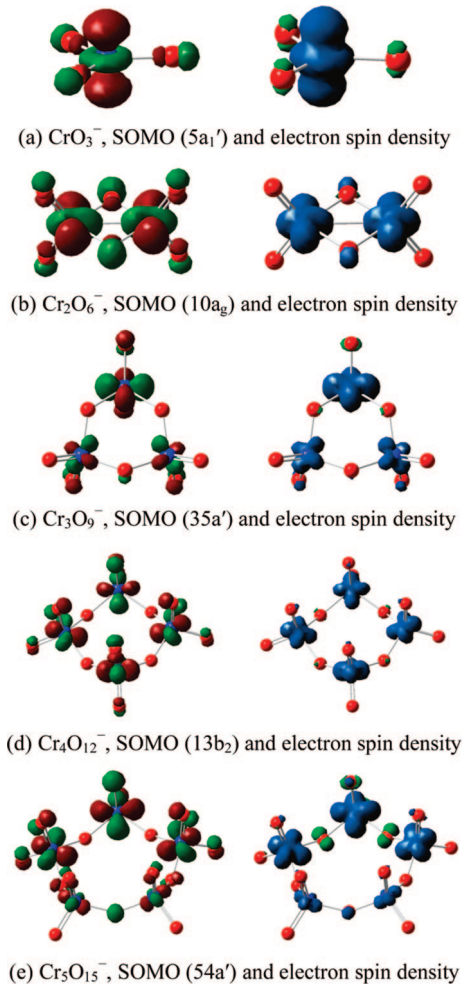

Figure 7. The singly occupied molecular orbitals (SOMO) and the electron spin density for the ground states of $(CrO_3)_n^-$ (n = 1–5).

lending additional support for the nonplanar structures identified in the current study.

6.3. Evolution of Electronic Structure and Energy Gap as a Function of Size. The PES pattern of $(CrO_3)_n^-$ (n = 1–5) as shown in Figure 1 is characteristic of a closed-shell neutral species with a sizable HOMO–LUMO energy gap.[18–20] The simplest electronic structure consideration of the $(CrO_3)_n$ clusters starts with a +6 charge on Cr and a −2 charge on O. The Cr−O bonding is substantially ionic with some covalent character due to charge redistribution, as demonstrated in our previous work of sequential oxidation in $Cr_2O_n^-$ (n = 1–7).[13] In bulk CrO_3, the O 2p orbitals form the valence band, whereas the Cr s and d orbitals form the conduction band. The energy difference between the valence band and conduction band defines the bulk band gap. The X−A energy gap of $(CrO_3)_n$ (n = 1–5) as tabulated in Table 2, which is defined as the ADE difference of the Cr 3d-based band X and the O 2p-based band A, can be considered to be a molecular analogue of the bulk band gap.

As shown in Table 1, the ADEs of band X range from 3.66 to 4.80 eV. The values are comparable to or substantially higher than those of the 4d and 5d congeners,[52,53] consistent with the contracted 3d orbitals of the first row transition metals with respect to the 4d and 5d transition metals.[54] The electron affinity increases sharply (by 0.59 eV) only from CrO_3 to Cr_2O_6 beyond which it increases almost linearly with a much smaller slope of 0.17–0.19 eV per CrO_3 unit from Cr_2O_6 to Cr_5O_{15} (Figure 2a), suggesting that electron delocalization on two metal centers is the primary reason for the additional stabilization of the extra electron going from CrO_3 to Cr_2O_6. The constant increase going to larger n suggests that the orbitals which the extra electron occupies for n = 2−5 are similar in nature and that the increased delocalization is responsible for the increasing stability of the anion relative to the neutral (Figure 7).

The ADE of band A also shows a large increase (by 1.23 eV) from CrO_3^- to $Cr_2O_6^-$, and the increase becomes smaller from $Cr_2O_6^-$ to $Cr_5O_{15}^-$ (0.20–0.53 eV per CrO_3 unit). As shown in Figure 2a, the ADE for band A increases faster than that for band X, thus opening up the energy gap with increasing cluster size (Figure 2b). Interestingly, the HOMO–LUMO gap seems to level off at n = 4 and reaches an asymptotic value of ~2.2 eV. Although the bulk CrO_3 crystal is structurally well-characterized,[51] its optical properties remain surprisingly elusive. Three widely different band gap values of 2.25, 3.14, and 4.32 eV have been reported.[55,56] The first two values were measured by reflectance spectra,[55] whereas the last value was obtained from electrical conductivity measurements.[56] The main experimental difficulty with the band gap measurements is that chromium forms various stable and intermediate oxide phases.[57] These phases include the three principal oxides CrO_3, CrO_2, and Cr_2O_3, which show distinct crystal structures and should lead to very different electronic and optical properties, but are readily interchangeable (e.g., via changes in temperature). The current cluster result suggests that the smaller value reported for the bulk may be closer to the true band gap for the bulk CrO_3 crystal.

7. Conclusions

We report a combined photoelectron spectroscopy and benchmarking density functional theory study on a series of chromium oxide clusters: $(CrO_3)_n$ and $(CrO_3)_n^-$ (n = 1–5). Well-resolved photoelectron spectra are obtained for $(CrO_3)_n^-$ (n = 1–5) and compared with extensive DFT calculations. Unique nonplanar cyclic ring structures are firmly established for $(CrO_3)_n$ and $(CrO_3)_n^-$ for $n \geq 3$. The structures can be described as formed from corner-sharing tetrahedral CrO_4 units with two Cr=O μ-oxo bonds and two Cr−O bridge bonds. The structural parameters of the $(CrO_3)_n$ clusters are shown to converge rapidly to those of the CrO_3 bulk crystal. The extra electron in the $(CrO_3)_n^-$ anions is shown to be largely delocalized over all Cr centers, consistent with the relatively sharp PES bands and smaller reorganization energies. The ADEs are shown to increase rapidly from CrO_3^- (3.66 eV) to $Cr_2O_6^-$ (4.25 eV), beyond which the increase becomes much smaller and is nearly linear for $(CrO_3)_n^-$ (n = 2–5). The energy gap increases sharply for n = 1–3 and converges to an asymptotic value of ~2.2 eV,

(51) Stephens, J. S.; Cruickshank, D. W. *Acta Crystallogr. B* **1970**, *26*, 222.
(52) (a) Zhai, H. J.; Kiran, B.; Cui, L. F.; Li, X.; Dixon, D. A.; Wang, L. S. *J. Am. Chem. Soc.* **2004**, *126*, 16134. (b) Zhai, H. J.; Huang, X.; Cui, L. F.; Li, X.; Wang, L. S. *J. Phys. Chem. A* **2005**, *109*, 6019.
(53) Huang, X.; Zhai, H. J.; Kiran, B.; Wang, L. S. *Angew. Chem., Int. Ed.* **2005**, *44*, 7251.
(54) See for example, the WebElements Periodic Table: http://www.webelements.com. The orbital radii of the d valence shell for Cr, Mo, and W are 45.5, 72.9, and 77.6 pm, respectively.
(55) Hanafi, Z. M.; Ismail, F. M.; Mohamed, A. K. *Z. Phys. Chem.* **1996**, *194*, 61.
(56) Khilla, M. A.; Hanna, A. A. *Thermochim. Acta* **1981**, *51*, 335.
(57) Kubota, B. *J. Am. Ceram. Soc.* **1961**, *44*, 239.

which is very close to the lower value reported for the bulk CrO_3 band gap.

Acknowledgment. This work was supported by the Chemical Sciences, Geosciences and Biosciences Division, Office of Basic Energy Sciences, U.S. Department of Energy (DOE) under Grant No. DE-FG02-03ER15481 (catalysis center program) and was performed, in part, in the W. R. Wiley Environmental Molecular Sciences Laboratory including the Molecular Science Computing Facility, a national scientific user facility sponsored by DOE's Office of Biological and Environmental Research and located at the Pacific Northwest National Laboratory, operated for DOE by Battelle. D.A.D. also thanks the Robert Ramsay Chair Fund of The University of Alabama for support.

Supporting Information Available: Cartesian coordinates optimized for $(CrO_3)_n$ and $(CrO_3)_n^-$ ($n = 1–5$), bond lengths and bond angles calculated for the ground electronic state of $(CrO_3)_n^-$ ($n = 1–5$) and different excited states of CrO_3 and Cr_2O_6 clusters, and harmonic vibrational frequencies for the $(CrO_3)_n$ and $(CrO_3)_n^-$ ($n = 1–5$) clusters, all at the PW91/aD level; additional excitation energies for $(CrO_3)_n$ ($n = 1–5$) calculated with the TD-DFT method at the anionic geometries; a figure showing the Franck–Condon simulation of the photoelectron spectrum for $Cr_2O_6^-$; and the complete refs 36, 38, and 39. This material is available free of charge via the Internet at http://pubs.acs.org.

JA077984D